applied sciences

MDPI

Article

Analysis of Bone Microstructural Changes Using Raman Spectroscopy in Women with Varus Deformity of the Knee Joint in the Course of the Primary Osteoarthritis

Paweł Kasprzak [1,*], Mirosław Szybowicz [2] and Maciej Głowacki [3]

[1] Department of Orthopedics and Traumatology of the Locomotor System, Hospital in Puszczykowo, Kraszewskiego 11 St., 62-041 Puszczykowo, Poland
[2] Department of Optical Spectroscopy, Faculty of Materials Science and Technical Physics, Poznań University of Technology, Piotrowo 3A St., 61-138 Poznań, Poland
[3] Department and of Pediatric Orthopedics and Traumatology, Poznań University of Medical Sciences, Fredry 10 St., 61-701 Poznań, Poland
* Correspondence: pw.kasprzak@gmail.com; Tel.: +48-510559593

Abstract: The aim of this study was to determine the correlation between the level of deformation, the degeneration rate of the knee joint, and the change in the structure of the subchondral bone layer affected by osteoarthritis in women. The study included patients diagnosed with primary knee osteoarthritis, with varus of the joint, planned for surgical treatment in the form of knee arthroplasty. The patients underwent a clinical and radiological assessment using standard radiographs of the knee joints in the anterior–posterior and lateral positions, while the level of varus deformity of the joint was determined on the basis of measurement radiographs of the lower limbs. Cartilage and bone materials from the tibial plateau were collected from 30 patients during the surgical treatments; these were then processed and examined using the Raman spectroscopy technique at the Department of Optical Spectroscopy of the Poznań University of Technology using the Renishaw inVia micro-Raman system coupled with a confocal microscope. The obtained Raman scattering spectra were analyzed by measuring the individual band intensities, and the results in the form of the ratios of selected Raman bands assigned to selected chemical groups were expressed as the mineralization index. The patients were divided into two groups, the first with a joint varus range of 3–10 degrees and the second with a range of 11–30 degrees. The patients were also divided into four groups, depending on the osteoarthritis degree, using the Kellgren–Lawrence scale. The investigation indicated that there is a relationship between the level of deformation and degeneration of the knee joint, expressed in scales based on radiological examination, and the coefficient, which determines the changes in the bone microstructure. The results showed that a decrease in mineralization occurred in the medial and lateral condyles as the knee osteoarthritis progressed. This study confirmed that the Raman spectroscopy technique is a useful tool for further research regarding the pathogenesis and course of osteoarthritis and may have an impact on the early diagnosis and treatment of knee osteoarthritis.

Keywords: knee osteoarthritis; mineralization index; Raman spectroscopy; subchondral bone

Citation: Kasprzak, P.; Szybowicz, M.; Głowacki, M. Analysis of Bone Microstructural Changes Using Raman Spectroscopy in Women with Varus Deformity of the Knee Joint in the Course of the Primary Osteoarthritis. *Appl. Sci.* **2023**, *13*, 2267. https://doi.org/10.3390/app13042267

Academic Editor: Hanatsu Nagano

Received: 19 December 2022
Revised: 4 February 2023
Accepted: 7 February 2023
Published: 10 February 2023

1. Introduction

Knee osteoarthritis is one of the main causes of chronic pain, and more advanced stages of this disease permanently impair the musculoskeletal system, as well as the functioning of patients. In its essence, it is primarily a disturbance of the balance between the process of degeneration and regeneration of the articular cartilage, involving overgrowth of the subchondral bone layer and the formation of osteophytes, which leads to a gradual impairment of joint function [1].

Primary knee osteoarthritis is the destruction of articular cartilage in conjunction with excessive thickening of the subchondral bone layer, the formation of osteophytes, and the

deformation of the affected joint (Figure 1) [2]. Primary osteoarthritis affects the medial tibiofemoral compartment in over 95% of cases. However, despite the known clinical course of the disease, the etiology and risk factors in primary osteoarthritis have not been fully elucidated [3].

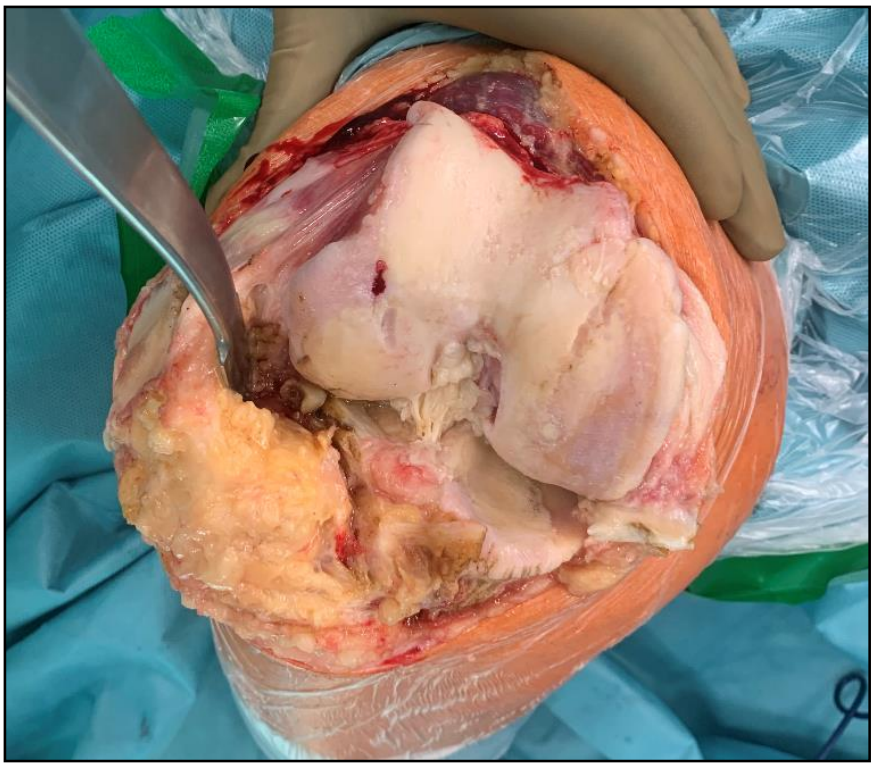

Figure 1. Osteoarthritis of the knee joint; in the upper part of the figure, femoral condyles are seen with major osteoarthritic changes. In the lower part, the tibial plateau (partially) is seen. Source: proprietary material, intraoperative photograph.

Imaging diagnostics of knee osteoarthritis cover a spectrum of tests, including X-ray diagnostics, ultrasonography, computed tomography, and magnetic resonance imaging. Knee arthroscopy, which allows the direct visualization of the internal structures of the joint due to the development of other diagnostic methods, is a surgical method that is currently primarily used to treat diseases and injuries of the knee joint. The assessment of osteoarthritis during surgical arthroscopy occurs simultaneously with treatment procedures. Each of the diagnostic methods has limitations due to their specificity, exposure to radiation, high costs, or limited availability.

According to the classification of Kellgren, Lawrence, and Crofty-Lane, a classic X-ray examination, which is most often performed in anterior–posterior and lateral projections, defines the disease at the stage of advanced cartilage defects, which lead to secondary changes in the joint (Figure 2).

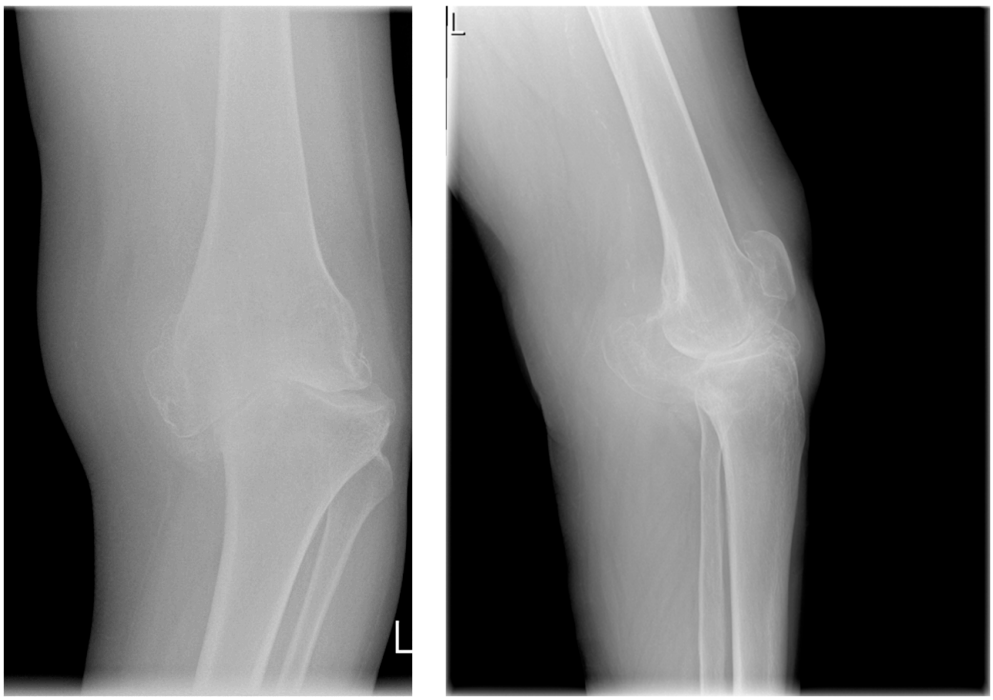

Figure 2. Osteoarthritis of the left knee joint, stage 4 on the Kellgren–Lawrence scale. Advanced destruction of the medial condyle of the femur (upper part) and tibia (lower part). Roentgenograms in AP (**left**) and lateral positions (**right**). Source: proprietary material.

Computed tomography is not considered the gold standard for the diagnosis of early degenerative changes due to exposure to ionizing radiation. Magnetic resonance maps the articular cartilage with increasing precision; however, the examination is expensive, and its availability is still limited. Currently, the development of a technology called delayed gadolinium-enhanced MRI of cartilage (dGEMRIC) is a step forward, as it makes it possible to non-invasively obtain biochemical and biophysical information regarding the surface of the articular cartilage [4]. However, the availability of this examination is low, and limitations are still created by the MRI's lack of sufficient resolution [5].

Vibrational spectroscopy is a tool used both to study the microstructure of biological material and as a diagnostic method that allows the analysis of the structures and processes that occur in the tissue [6]. Infrared spectroscopy and Raman spectroscopy can be applied to determine subtle changes in bone tissue as remineralization processes or the disorganization of collagen fibers. The use of vibrational spectroscopy to analyze the structure and changes within bones, cartilage, or enamel began to play an important role in research regarding the quantitative and qualitative composition of tissues [7,8].

The effectiveness of Raman spectroscopy in the analysis of the composition of biological material, including bones, has been confirmed by many studies [9–12] and allowed us to determine a specific "footprint" of the individual chemical compounds present in the bone tissue [13,14]. Based on the knowledge regarding the location of individual bands of the spectrum and the fact that the positions of the bands are constant, both qualitative and quantitative analyses of chemical compounds are possible in the study.

The main bands of the Raman spectrum of the subchondral bone layer and cancellous bone relate to the wave number corresponding with the vibrations of phosphates, carbonates, and organic matrices of amide I, amide III, and C-H stretching bonds. For the analysis of Raman spectra, the intensity ratios of integral bands related to specific wave numbers, i.e., oscillatory vibrations, were used. These ratios allow the determination of the bone mineralization index (MI). This indicator was established on the basis of determining the ratio of the intensity of the integral phosphate bands ν_1 to the intensity of the amide III bands (ν_1 PO_4^{3-}/amide III) within the vibration range of 960–961 cm^{-1} for the phosphate

groups and 1243–1300 cm^{-1} for amide bonds III [15]. The above-mentioned parameter is widely used in studies in which Raman spectroscopy is applied for the study of bone tissue in order to analyze the change in bone composition as the ratio of minerals to the matrix and the shift of these phases in favor of the mineral or organic phase [16].

It was assumed that changes in the bone microstructure would occur along with the progress of deformation and the degree of degeneration.

Significant research on distinguishing between non-infected human bone samples and Staphylococcus epidermidis-infected bone samples by Raman measurements was recently conducted. A substantial loss in bone quality and protein conformation was detected by human bone samples co-cultured with *Staphylococcus epidermidis*. Substantial changes were detected in the mineral-to-matrix ratio, carbonate-phosphate ratio, alterations in the collagen network, and a decrease in the collagen structural organization [17].

The aim of this study was to correlate the mineralization index of the subchondral bone layer depending on the degree of degenerative changes expressed on the Kellgren–Lawrence scale and the level of varus deformity occurring in primary knee osteoarthritis in women [18].

2. Materials and Methods

2.1. Materials

2.1.1. Participants

Patients diagnosed with primary knee osteoarthritis qualified for surgical treatment in the form of endoprosthesoplasty of the knee joint and underwent clinical and radiological assessment and determination of the level of varus deformity of the joint. Patients with a secondary form of osteoarthritis (post-traumatic, related to rheumatic diseases, with a history of knee-joint surgery) were excluded from the study.

Patients were qualified according to the waiting list for surgery.

The patients underwent imaging diagnostics: X-rays in the anterior–posterior and lateral positions, as well as measurement images on a long film, were obtained. The course of the research is shown in Scheme 1.

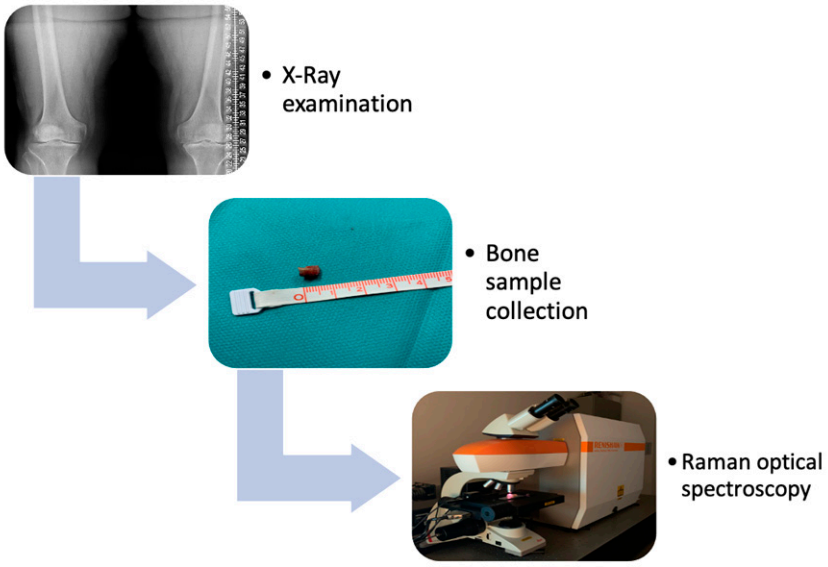

Scheme 1. Graphical course of research.

2.1.2. Bone Material Collection

Material from the tibial plateau was collected during knee arthroplasty. The samples were then processed in the form of 5 × 5 mm cartilage–bone blocks, according to a technique previously used by other researchers [19]. Bone blocks were prepared using the oscillating microsaw, usually used for small bone osteotomy.

The collection of cartilage and bone material did not extend the scope of the operation. It was one of the stages of the surgical treatment in accordance with the surgical technique. The patients were informed about the course of the operation and the collection and preservation of the material before qualifying for the study and immediately before the procedure.

2.1.3. Raman Microscopic Spectroscopy

The prepared bone blocks in the form of 180 samples were further analyzed in the spectroscopic laboratory at the Department of Optical Spectroscopy of the Poznań University of Technology.

2.1.4. Bioethical Commission

The study was conducted in accordance with the Declaration of Helsinki and approved by the Bioethical Commission at the Poznań University of Medical Sciences no. 1199/17 on 7 December 2017.

2.2. Methods

2.2.1. X-ray Imaging and Radiological Arthritis Classification

The patients underwent radiological assessment in accordance with generally accepted standards of radiological diagnostics. Based on the radiographs taken in the anterior–posterior and lateral positions, the severity of the osteoarthritis was determined on the Kellgren–Lawrence scales (Figure 3). On the first scale, patients were assigned to the appropriate degree of osteoarthritis, from grade 0 to 4.

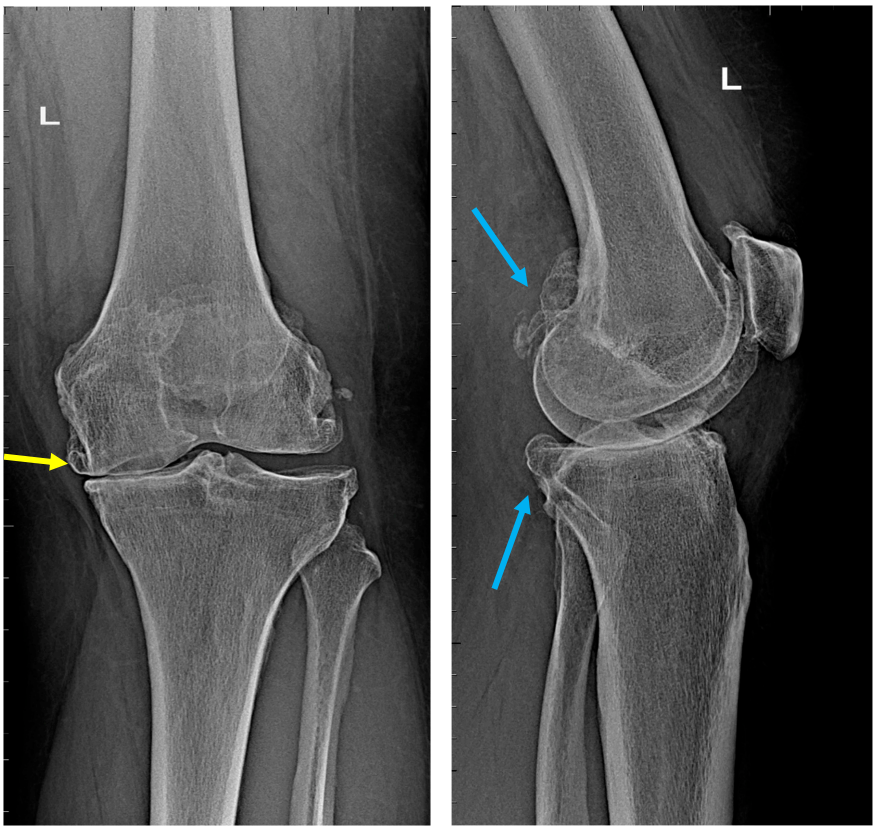

Figure 3. Radiographs of the knee joint. Grade-4 arthrosis on the K–L scale, grade 3 on the Crofty-Lane scale. **Left**—AP view, **right**—lateral view. Visible (yellow arrow) complete narrowing of the joint space in the medial compartment, numerous osteophytes (blue arrows), and joint-axis disorders. Upper part: femoral bone, lower part: tibia and fibula. Source: proprietary material.

2.2.2. X-ray Measurement of the Lower Limb Axis

In the second stage of the radiological assessment, the mechanical axis of the operated lower limb was plotted. The measurement was carried out using radiological pictures on a long measuring film in a digital form. The measurement was conducted in a standing position, with a full load on the limbs. The radiological examination covered the anatomical area from the iliac plates to the feet, with the necessary consideration of the heads of the femurs and blocks of the talus on both sides, as shown in Figure 4.

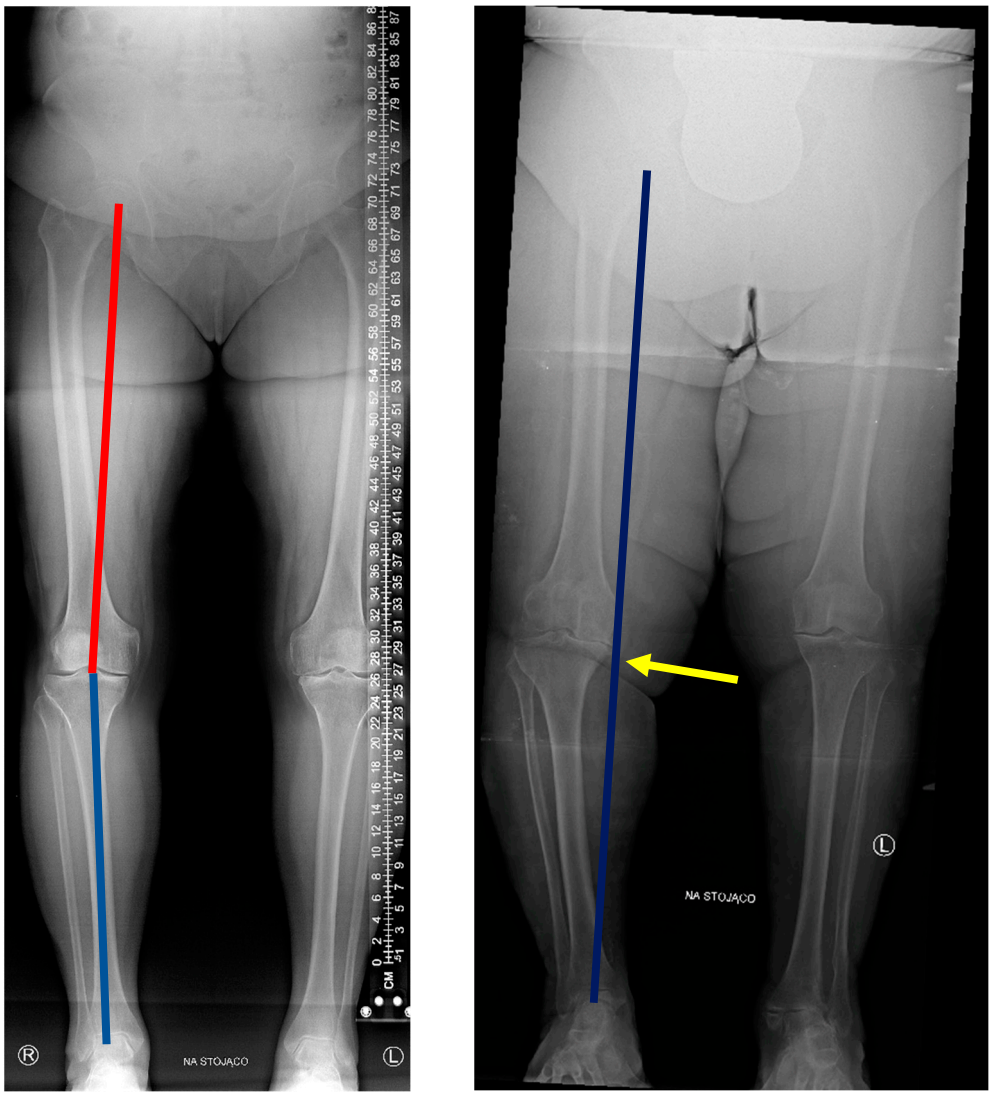

Figure 4. Measurement X-ray of the lower limbs in a patient with a slight varus deformity of the knee joint (**left**) and an advanced deformity (**right**). On the left, HKA angle is presented: red line shows hip–knee line; blue line shows knee–ankle line. On the right: narrowing of the medial compartment (yellow arrow) affecting the mechanical axis of the limb (blue line). The line moved medially indicates varus deformity of the knee joint. Source: proprietary material (description "na stojąco" [pl] means in the weightbearing position).

The measurements were carried out using the method of plotting the mechanical axis of the lower limb, using the HKA angle, with the classification of varus deformity used in The Journal of Arthroplasty [20], in which the HKA angle equal to and lower than 177° is considered to be a varus deformity of the joint, divided into stages. For the sake of clarity, the degree of deformation is defined as the angle complementary to the angle of 180°. Below 3°, the result was normal; a value in the range of 4°–10° is considered a slight deformation. In the range of 11°–20°, the deformation is defined as notable. Significant

deformation occurs in the range of 21°–30°, while beyond 30°, the deformation is defined as extreme.

The exact measurement of the axis of the lower limb was determined in accordance with the previously presented classification. The measurement was conducted by marking a line running from the center of the femoral head to the knee joint and from the center of the knee joint to the center of the talus block, followed by measuring the angle between the marked lines and assigning it to the appropriate angle HKA, described above (Figure 4).

Due to the notable differences in the destruction of cartilage and bone tissue, the patients were divided into 2 groups for the purposes of this study based on the deformity of the knee joint: mild varus deformity and advanced varus deformity.

Patients from the slight deformity group, i.e., 4°–10° HKA angle, were qualified for the mild deformity group.

The group of advanced deformities included patients with an HKA angle of 11°–30° degrees, described as a notable and significant deformity. The tibial plateau in deformities exceeding 30 degrees was characterized by complete destruction of the medial condyle; hence, it was impossible to collect the bone block. At this degree of deformity, it was also not possible to use a standard primary tibial implant.

Ultimately, 15 patients were qualified for both comparative groups.

2.2.3. Sample Collection and Preparation

Immediately before the Raman spectroscopy examination, the samples were thawed under laboratory conditions. The prepared sample is shown in Figure 5. They were then cut to 5 × 5 mm blocks successively from the anterior, middle, and posterior parts of the medial tibial condyle (AMC, MMC, PMC) and the anterior, middle, and posterior parts of the lateral tibial condyle (ALC, MLC, PLC). The technique proposed by Y. Takahashi was used to determine the location of the bone block collection, in case of which the sample corresponding to the center of the medial condyle marked as MMC falls on the most loaded surface, after which the AMC sample corresponds to the anterior part of the condyle and the PMC sample to its posterior part. The donor sites within the lateral condyle of the tibia were marked similarly.

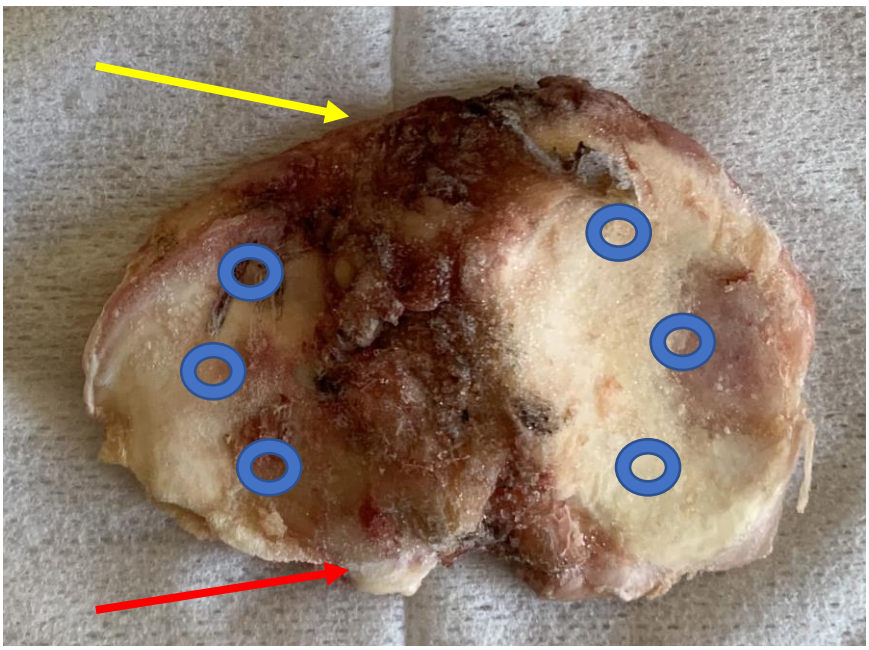

Figure 5. Prepared tibial condyle. Yellow arrow—anterior part of the condyle; red arrow—posterior part of the condyle. Blue rings—places of the bone blocks collection. Source: proprietary material.

2.2.4. Raman Microscopic Spectroscopy

The Renishaw inVia micro-Raman system (UK), equipped with a Leica confocal microscope, was used for spectroscopic studies. A laser operating at a wavelength of 785 nm was used as the excitation light source. The ×50 long working distance (CCD) lens was used in the study.

During the microspectroscopic study, the Raman spectral region of the bone subchondral tissue was obtained in the spectral range of 200–1800 cm^{-1} (Figure 6). Each wave number corresponds with the defined vibration type (Table 1). The study was conducted by averaging the results of 3 measurements: measurement at a microscopically determined point in the middle part of the designated block and points 10 µm above and below this point. Measurements not meeting the physical or qualitative testing standards were repeated. The obtained results were compared with the previously obtained data: the degree of knee-joint degeneration and varus deformity of the joint.

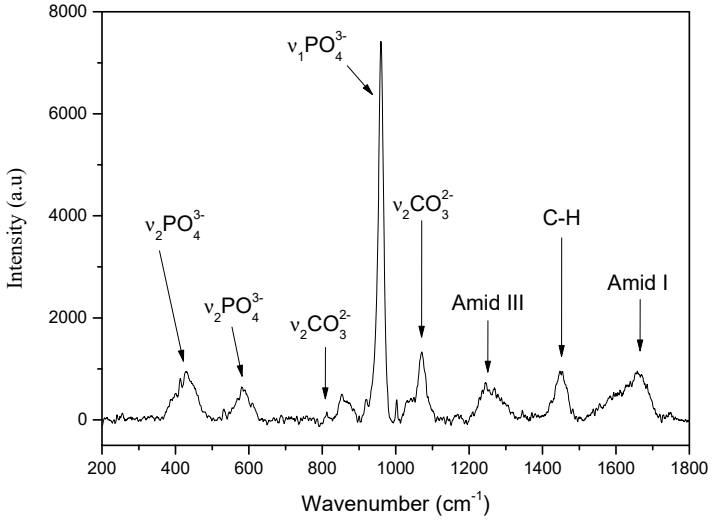

Figure 6. Raman scatter spectrum obtained for the subchondral bone tissue. Source: materials belonging to the Department of Optical Spectroscopy of the Poznań University of Technology.

Table 1. Location of the corresponding bands in the Raman scattering spectrum.

Wave Number (cm^{-1})	Vibration Type
430–450	ν_2 PO_4^{3-}
587–604	ν_4 PO_4^{3-}
855–857	Proline
960–961	ν_1 PO_4^{3-}
1003	Phenylalanine
1003	HPO_4^{2-}
1035–1048	ν_3 PO_4^{3-}
1070–1075	ν_1 CO_3^{2-} type B
1103	ν_1 CO_3^{2-} type A
1243–1253	Amide III—a statistical bundle
1265–1300	Amide III—alpha helix
1400–1470	C-H bending
1595–1700	Amide I
2800–3100	C-H stretching

The spectroscope used for the research works in back-scattering geometry. The spectroscope is used in a classical light-scattering system.

2.2.5. Data Processing

The mineralization index, measured as the ratio of the phosphate group to spectrum to the amide III band, reflects the level of mineralization of the subchondral bone layer. The examined points were compared based on the level of deformation.

To check the significance of the difference between the two groups, the following were used:

- Student's *t*-test if the conditions of normality of distribution and homogeneity of variance are met;
- The Cochran–Cox test if the condition of the normal distribution is met and the variance is not homogeneous;
- The Mann–Whitney U-test in the case of non-normal distribution.

Subsequently, the mineralization indices were compared based on the degree of the knee-joint degeneration on the Kellgren–Lawrence scale using ANOVA analysis:

- ANOVA (analysis of variance)—if the condition of the normality of distribution and the condition of homogeneity of variance were met;
- Welch's ANOVA—in the case of meeting the condition of normal distribution and not meeting the condition of homogeneity of variance;
- Kruskal–Wallis ANOVA—in the case of failure to meet the condition of normal distribution.

The value of $p < 0.05$ was considered statistically significant. Statistical calculations were performed using the STATISTICA 10 PL statistical package.

3. Results

Table 2 shows information about patients' statistics, including age and BMI (kg/m^2).

Table 2. Patients' statistics information.

Variable	n	Mean	Mean SD	Median	Min.	Max.
Age (years)	30	69.0	8.0	69.5	52	83
BMI (kg/m^2)	30	33.05	4.31	33.42	24.17	40.63

Statistically significant differences in the level of mineralization index between patients with mild deformity and patients with advanced deformity occurred for the anterior part of the medial condyle ($p = 0.0481$, Cochrana–Cox test), as seen in Figure 7. Changes were also observed in the medial part of the medial condyle ($p = 0.0133$, Student's *t*-test), as displayed in Figure 8.

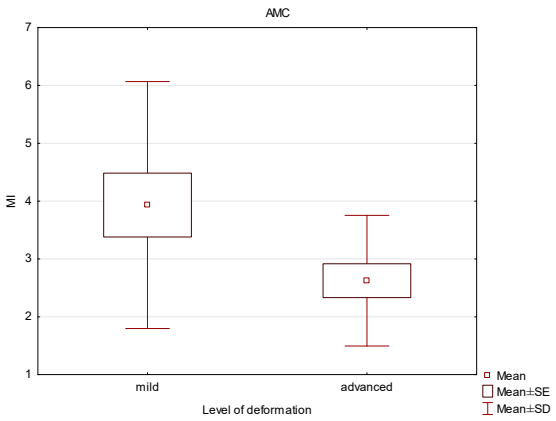

Figure 7. Box and whisker plot of the mineralization index (MI) in patients with mild and advanced deformity in the anterior part of the medial condyle (AMC).

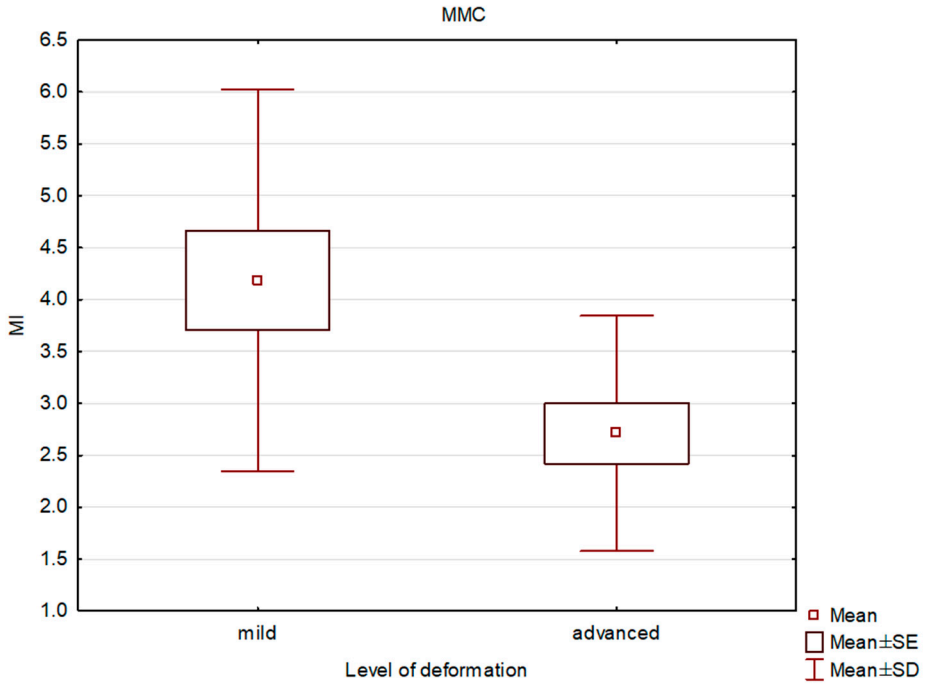

Figure 8. Box and whisker plot of the mineralization index (MI) in patients with mild and advanced deformity in the medial part of the medial condyle (MMC).

Similar mineralization changes were observed in the anterior part of the lateral condyle (p = 0.0251, Mann–Whitney U-test), as shown in Figure 9, and in the posterior part of the lateral condyle, presented in Figure 10 (p = 0.0442, Student's t-test).

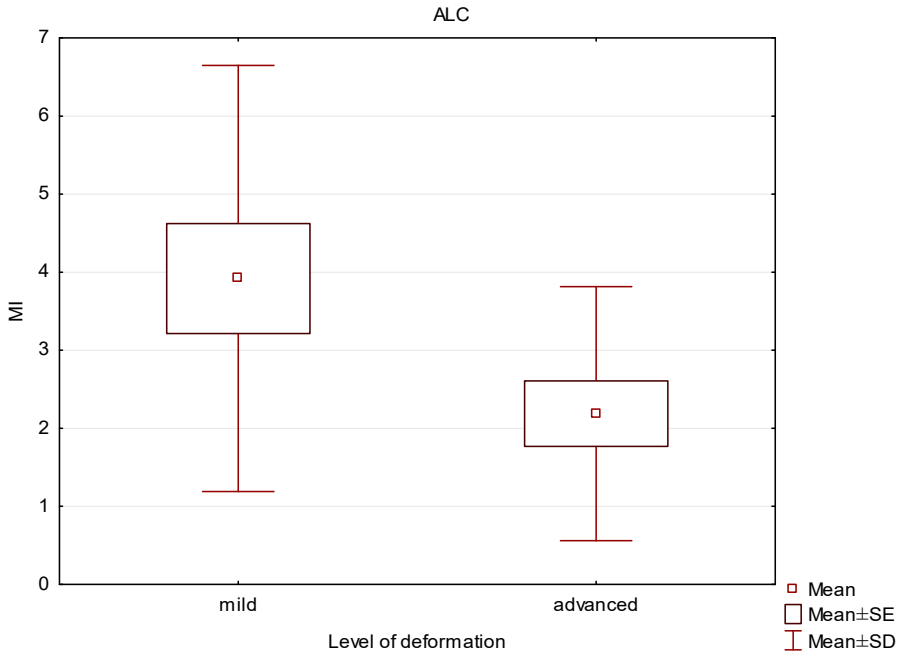

Figure 9. Box and whisker plot of the mineralization index (MI) in patients with mild and advanced deformity in the anterior part of the lateral condyle (ALC).

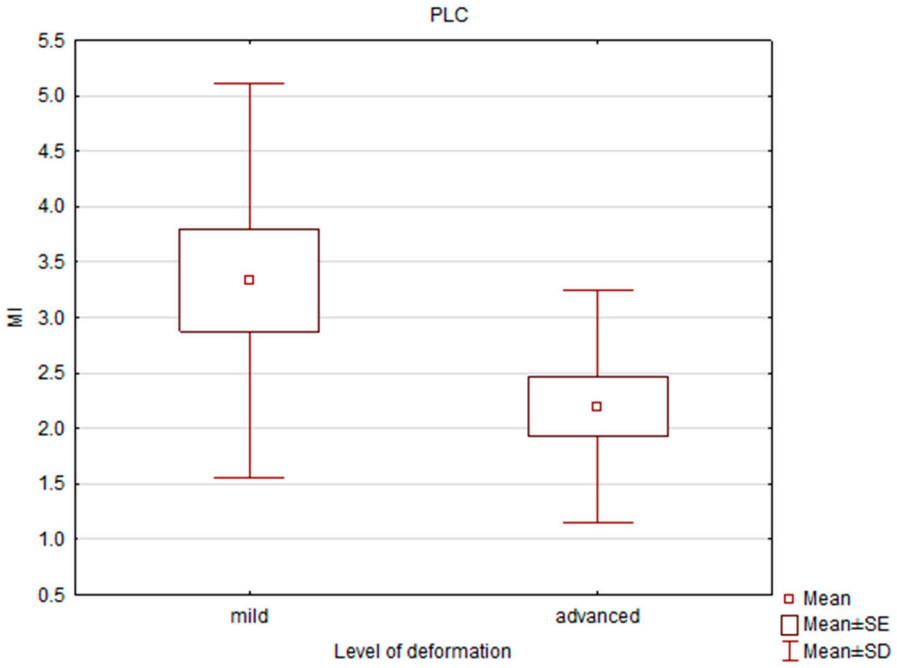

Figure 10. Box and whisker plot of the mineralization index (MI) in patients with mild and advanced deformity in the posterior part of the lateral condyle.

In both the medial and lateral condyles, there were statistically significant differences in the MI, which decreased with progressive varus deformity.

The average mineralization index decreased within one condyle as the deformity increased. Within the examined site, the MI decreased with the increase in the level of deformation. Greater differences were noticeable within the medial condyle ($p = 0.0278$, *t*-Student test), Figure 11, than in the lateral condyle ($p = 0.0426$, *t*-Student test), Figure 12. Within the medial condyle, the greatest changes occurred within the part with the greatest load, namely in the middle part of the condyle. Varus deformity also reduced the mineralization index in the lateral condyle; however, the extent of this change was lower. Ultimately, as the deformation progressed, the degree of bone mineralization decreased.

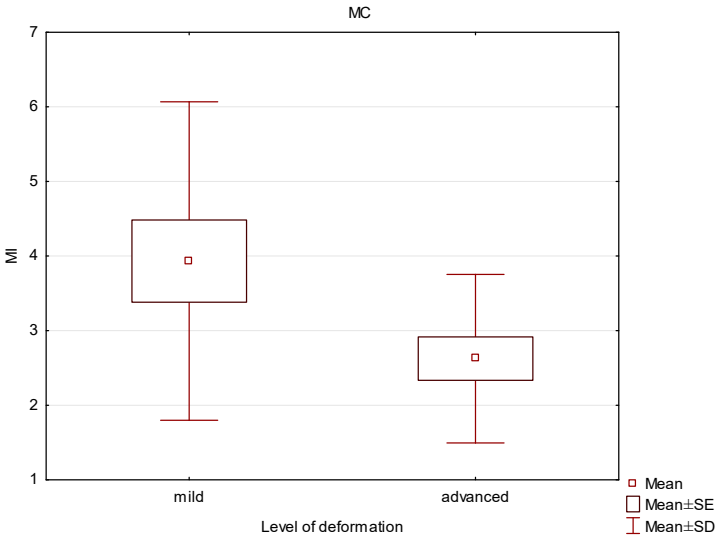

Figure 11. Box and whisker plot of the mineralization index (MI) in patients with mild and severe deformities in the medial condyle (MC).

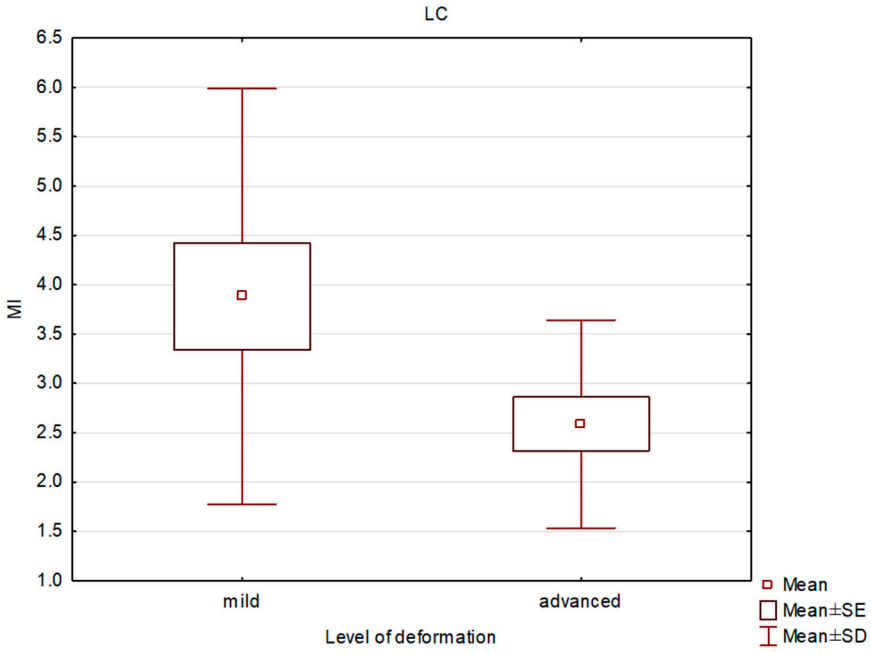

Figure 12. Box and whisker plot of the mineralization index (MI) in patients with mild and severe deformities in the lateral condyle (LC).

In the subsequent stages of degenerative changes, there was a decrease in the level of mineralization in both tibial condyles, as shown in Figure 13 (NIR post hoc test), referring to the medial condyle and Figure 14 (NIR post hoc test), referring to the lateral tibial condyle.

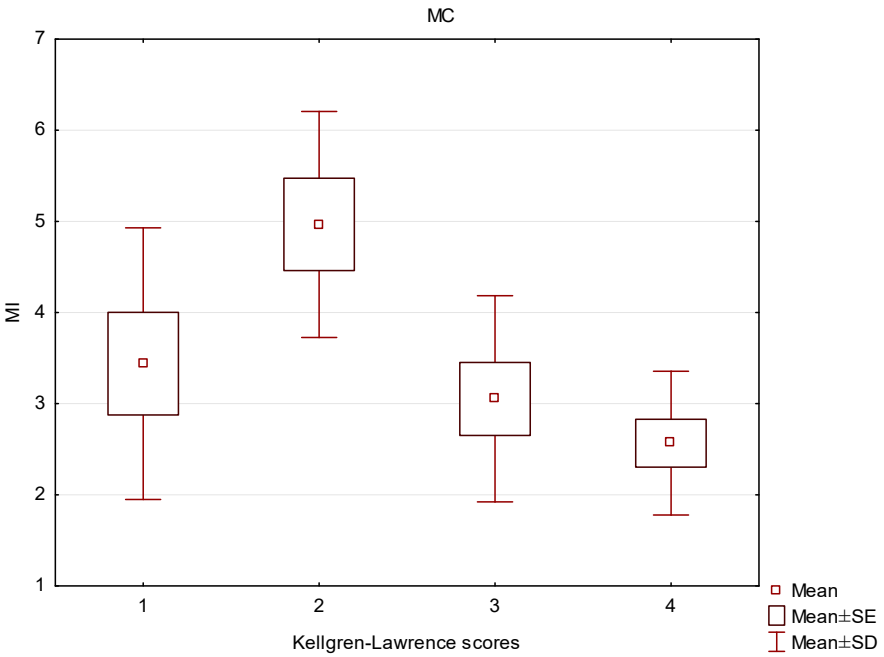

Figure 13. Box and whisker plot of the mineralization index (MI) in patients with different Kellgren–Lawrence scores in the medial condyle (MC).

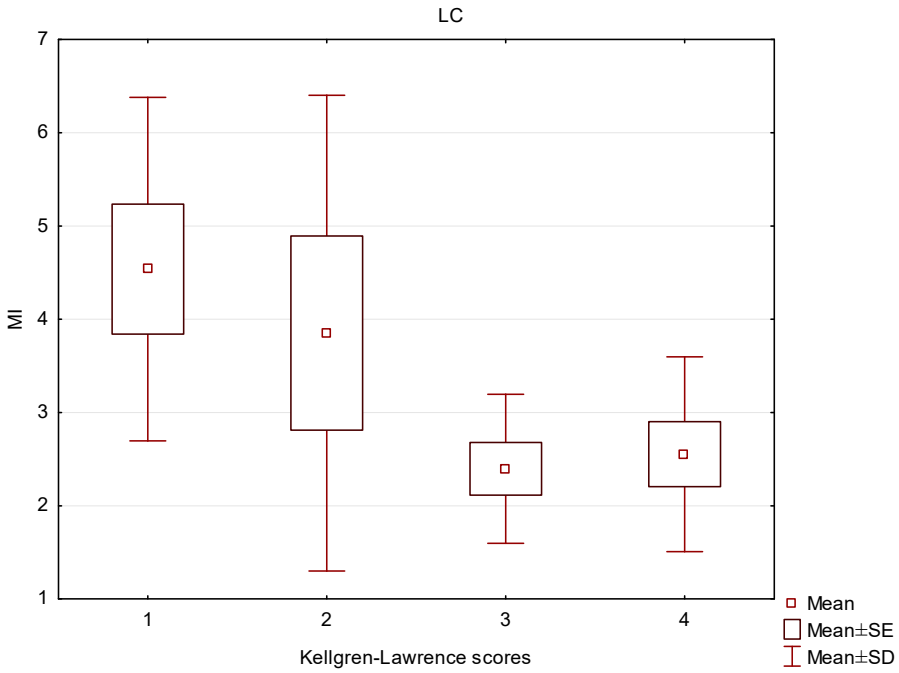

Figure 14. Box and whisker plot of the mineralization index (MI) in patients with different Kellgren–Lawrence scores in the lateral condyle (LC).

Within the examined areas of the medial condyle, there was a temporary increase in mineralization in grade 2 according to K-L; subsequently, in grades 3 and 4 on the K-L scale, there was an equal decrease in mineralization within both the medial and lateral condyles.

The changes in the indices examined in this study correlated with the stage of degenerative changes and the level of deformation of the limb axis. In the course of the study, it was confirmed that the change in the degree of osteoarthritis and the level of deformation was reflected in the bone microstructure. The examined bone mineralization indices depend on the degree of degeneration and the level of deformation.

Significant changes in the subchondral bone correlated with the degree of varus deformity of the limb. The mineralization index is an indicator that most reproducibly responds to changes in the structure of the subchondral bone layer, i.e., it is expressed by the ratio of the intensity of integral phosphate bands ν_1 to the intensity of amide III bands (ν_1 PO_4^{3-}/amide III) from the vibration areas of 960–961 cm^{-1} for phosphate groups and 1243–1300 cm^{-1} for amide bonds III. Its value decreased with the degree of deformity for all stages of varus deformity and for both condyles. In the case of mild varus deformity, the MI was similar, with a slight decrease in the medial condyle, while in advanced deformity, the decrease in MI was more pronounced in the medial than in the lateral condyle. This index indicates a decrease in bone mineralization—disturbance of the axis of the limb intensifies this process.

4. Discussion

4.1. Changes in Subchondral Bone

This study confirmed that the structure of the subchondral bone layer undergoes a number of changes, which intensify with the progression of varus and the degree of degeneration. The obtained research results are consistent with the studies of other researchers, which indicate bone remodeling of the subchondral bone layer along with the intensification of degenerative changes and deformation of the joint as a rationale for this process [21].

Significant research focused on evaluating the microstructural changes in bones, depending on the degree of articular cartilage damage and the degree of joint degeneration, was conducted by Kerns in 2014. Kern compared 10 designated areas of the tibial plateau

with the fourth degree of articular cartilage damage on the Outerbridge scale, with analogous areas within the tibial plateau with intact cartilage. The use of the Raman spectroscopy technique along with PCA (principal components analysis) and PCA-LADA (PCA—linear discriminant analysis) made it possible to distinguish material with features of arthrosis from material without signs of degeneration [22].

In the same study, the investigators demonstrated changes in subchondral bone mineralization with concomitant subchondral thickening during peripheral quantitative tomography (pQCT). The results of these studies indicate that the change within the subchondral zone of the bone is not only due to the thickening of the layer and that changes also occur at the microstructural level [23]. The research presented in this study includes similar observations. The study of samples according to the level of varus deformity in women, i.e., of samples from a homogeneous research group, allowed us to observe a transient increase in mineralization within the medial condyle, which may correspond to compensation due to the increasing load. Furthermore, the level of mineralization decreased equally and rapidly within both tibial condyles in the course of degenerative changes. It is also worth noting that in the study, based on the level of deformity, the MI was characterized by similar values for the medial and lateral condyles; the decrease in mineralization was also observed at a similar level.

It seems that the differences between the damage zones within the lateral and medial condyles depend on the anatomical conditions and the complexity of the movement in the knee joint, including translation and rotation, in addition to flexion and extension. In the works of other authors, the differences in the areas of articular cartilage damage are also described, which is reflected in [3].

Takahashi studied changes within the intensity band 1241–1269 cm^{-1} (amide III doublet), which is associated with the spatial conformation of type II collagen, a component of joint cartilage. The author conducted a study on the material of five tibias covered with degenerative disease and one tibia from a deceased donor without signs of degeneration. He described degenerative changes within the factor under study along with the progression of macroscopic cartilage damage [19]. The authors of the study focused on damage to the articular cartilage, but the results correspond with the research carried out in the subchondral bone.

One theory, introduced by Radin in 1972, is that the increased load on the joint leads to a gradual adaptation of the bone and results in a thickening of the subchondral layer. The new, more rigid structure is less effective at absorbing shocks and, thus, the distribution of forces transmitted by the affected joint changes. The next stage of the process involves secondary changes in the articular cartilage, the destruction of which deepens in places with the greatest load on the joint [2,23]. Considering the mechanical concept leading to secondary changes within cartilage and bone, the theory assumes that the newly formed bone does not exhibit changes in its chemical structure. In this study, it is noteworthy that the subchondral layer of the femur underwent a temporary increase in the degree of mineralization during the second degree of degeneration on the K-L scale. As a consequence, a further decrease in the level of mineralization may have been caused by the inability to further compensate for this process.

Other authors put emphasis on degenerative changes in the cartilage and bone as a result of connective tissue diseases in the course of collagen degeneration [24,25].

Therefore, with significant caution, it can be assumed that varus deformity of the knee joint is primarily related to mechanical factors and that changes in bone mineralization occur subsequently. The progression of changes in the chemical composition of the bones intensifies with the destruction of the joint surface. A similar correlation between articular cartilage damage and changes in the subchondral layer was also observed by researchers in other studies [26]. Other researchers even indicated a significant correlation between the mineralization of the subchondral bone layer and the level of joint-gap narrowing in their studies, defining the condition of the subchondral bone layer as a prognostic factor for the

progression of degenerative changes [27]. The research results presented in this study led to similar conclusions.

Pathological processes occurring in the skeleton at the developmental age also lead to changes in the structure of bone tissue and may later lead to a decrease in its strength [28,29].

4.2. Vibrational Spectroscopy in Biological Material

Vibrational spectroscopy is both a tool used to study the microstructure of biological material and a diagnostic method that allows the analysis of the structure and processes occurring in tissue and in the course of genetic mutations [6,30]. Infrared spectroscopy and Raman spectroscopy make it possible to determine changes in bone tissue as subtle as remineralization processes or the disorganization of collagen fibers. Starting from the research by Carden and Morris in 2000, the use of vibrational spectroscopy to analyze the structure and changes within bones, cartilage, or enamel began to play a significant role in research regarding the quantitative and qualitative composition of tissues [7,8].

This technique plays an increasingly important role as a diagnostic tool and supplements biochemical, imaging, and histological studies. Spectroscopy makes it possible to create maps, taking into account the chemical composition of healthy and pathologically changed tissue, as well as changes occurring in tissues between both above-mentioned states. Tissue changes result in new spectra, band shifts, or intensity changes.

The applied Raman spectroscopy method has an advantage over infrared spectroscopy, associated with only possibly minimal preparation of samples and lower sensitivity to the degree of tissue hydration, which is extremely important in the case of biological material, as it does not disturb the image of the obtained scatter spectra and makes it possible to conduct measurements at a higher spatial resolution [13,31]. As a result of the above-mentioned advantages, a considerable advantage of Raman spectroscopy is the possibility of using it in both in vivo and ex vivo models. The usefulness of spectroscopic examination, with particular emphasis on biological tissues, has already been described by researchers, and, at the same time, it allows the expansion of current research with qualitative and quantitative data regarding bone and cartilage composition [7]. This feature offers a new perspective on the possibility of conducting intraoperative assessments of cartilage and bone tissue, such as in osteoarthritis, as well as the diagnosis of pathological fractures or pathological changes in the skeleton at the developmental age.

4.3. Practical Value

The practical value of the research is to pay attention to the changes occurring within the subchondral bone layer in the course of degenerative disease. Taking into account the fact of lower mineralization and a decrease in the content of hydroxyapatite in the subchondral bone layer, it seems important to ask whether cementless knee arthroplasty in more advanced stages of osteoarthritis can provide a satisfactory and long-term therapeutic effect for the patient. It can be speculated that these changes may negatively affect the method of osseointegration of the endoprosthesis and accelerate the loosening process of the endoprosthesis. It should be noted that despite the clinical thickening of the subchondral bone layer and sclerosis visible in roentgenograms, this layer has a significantly changed microstructure. Studies show that patients should be qualified for single-compartment endoprosthesis with great caution when radiologically large changes occur in the subchondral bone layer at the same time.

The latest research demonstrates the potential of NIR spectroscopy coupled with a deep-learning approach as a means of rapid PMI classification of human bone samples. This approach can distinguish between forensic and archaeological human bone samples [32].

To summarize, in light of the presented studies, the bone mineralization index is the most useful parameter for imaging changes in the bone microstructure, and it is most sensitive to changes within unfixed bone tissue, as also indicated by the results of other authors, who used the range of 960–961 cm^{-1}, which corresponds to phosphorus groups. The ratio of carbonate apatite to hydroxyapatite also provides crucial information. Raman

spectroscopy opens up new analytical and diagnostic possibilities due to the possibility of examining unfixed preparations. The sensitivity of the method, which is not only limited to the presence or absence of degenerative changes, along with the ability to determine the progression or severity of such changes, increases its usefulness.

However, further clinical trials are necessary, which would enable the use of the method not only in degenerative disease but also in the diagnosis of necrotic bone, cancer diagnosis, or the possibility of predicting osteoporotic fractures.

Author Contributions: Conceptualization, P.K., M.G. and M.S.; methodology, M.G. and M.S.; software, M.S.; validation, P.K., M.S. and M.G.; formal analysis, P.K.; investigation, P.K.; resources, P.K.; data curation, P.K.; writing—original draft preparation, P.K.; writing—review and editing, P.K.; visualization, P.K.; supervision, M.G. and M.S.; project administration, M.G. and M.S.; funding acquisition, P.K. All authors have read and agreed to the published version of the manuscript.

Funding: This research received no external funding.

Institutional Review Board Statement: The study was conducted in accordance with the Declaration of Helsinki and approved by the Bioethical Commission at the Poznań University of Medical Sciences no. 1199/17 on 7 December 2017.

Informed Consent Statement: Informed consent was obtained from all subjects involved in the study.

Data Availability Statement: The data presented in this study are available on request from the corresponding author. The data are not publicly available due to the patients' data.

Acknowledgments: The material was collected during the surgical procedure in the Hospital of Puszczykowo. Samples were prepared at the Poznań University of Medical Sciences. All the measurements were carried out using a Renishaw inVia microscope at the Poznan University of Technology.

Conflicts of Interest: The authors declare no conflict of interest.

References

1. Martel-Pelletier, J. Pathophysiology of osteoarthritis. *Osteoarthr. Cartil.* **2004**, *12*, 31–33. [CrossRef] [PubMed]
2. Radin, E.L. Who gets osteoarthritis and why? *J. Rheumatol. Suppl.* **2004**, *70*, 10–15. [PubMed]
3. Nakagawa, Y.; Mukai, S.; Yabumoto, H.; Tarumi, E.; Nakamura, T. Cartilage Degeneration and Alignment in Severe Varus Knee Osteoarthritis. *Cartilage* **2015**, *6*, 208–215. [CrossRef] [PubMed]
4. Bron, E.E.; van Tiel, J.; Smit, H.; Poot, D.H.J.; Niessen, W.J.; Krestin, G.P.; Weinans, H.; Oei, E.H.G.; Kotek, G.; Klein, S. Image registration improves human knee cartilage T1 mapping with delayed gadolinium-enhanced MRI of cartilage (dGEMRIC). *Eur. Radiol.* **2013**, *23*, 246–252. [CrossRef] [PubMed]
5. Glover, P.; Mansfield, S.P. Limits to magnetic resonance microscopy. *Rep. Prog. Phys.* **2002**, *65*, 1489–1511. [CrossRef]
6. Buchwald, T.; Kozielski, M.; Szybowicz, M. Determination of Collagen Fibers Arrangement in Bone Tissue by Using Transformations of Raman Spectra Maps. *Spectrosc. Int. J.* **2012**, *27*, 107–117. [CrossRef]
7. Carden, A.; Morris, M.D. Application of vibrational spectroscopy to the study of mineralized tissues (review). *J. Biomed. Opt.* **2000**, *5*, 259–268. [CrossRef]
8. McCreadie, B.R.; Morris, M.D.; Chen, T.; Rao, D.S.; Finney, W.F.; Widjaja, E.; Goldstein, S.A. Bone tissue compositional differences in women with and without osteoporotic fracture. *Bone* **2006**, *39*, 1190–1195. [CrossRef]
9. Bi, X.; Patil, C.A.; Lynch, C.; Pharr, G.M.; Mahadevan-Jansen, A.; Nyman, J.S. Raman and mechanical properties correlate at whole bone and tissue levels in a genetic mouse model. *J. Biomech.* **2011**, *44*, 297–303. [CrossRef]
10. Carter, E.A.; Tam, K.K.; Armstrong, R.S.; Lay, P.A. Vibrational spectroscopic mapping and imaging of tissues and cells. *Biophys. Rev.* **2009**, *1*, 95–103. [CrossRef]
11. Morris, M. Raman Spectroscopy of Bone and Cartilage. In *Emerging Raman Applications and Techniques in Biomedical and Pharmaceutical Fields*; Matousek, P., Morris, M., Eds.; Springer: Berlin/Heidelberg, Germany, 2010; pp. 347–364.
12. Nyman, J.S.; Makowski, A.J.; Patil, C.A.; Masui, T.P.; O'Quinn, E.C.; Bi, X.; Guelcher, S.A.; Nicollela, D.P.; Mahadevan-Jansen, A. Measuring Differences in Compositional Properties of Bone Tissue by Confocal Raman Spectroscopy. *Calcif. Tissue Int.* **2011**, *89*, 111–122. [CrossRef] [PubMed]
13. Penel, G.; Delfosse, C.; Descamps, M.; Leroy, G. Composition of bone and apatitic biomaterials as revealed by intravital Raman microspectroscopy. *Bone* **2005**, *36*, 893–901. [CrossRef] [PubMed]
14. Raghavan, M.; Sahar, N.; Wilson, R.; Mycek, M.-A.; Pleshko, N.; Kohn, D.H.; Morris, M.D. Quantitative polarized Raman spectroscopy in highly turbid bone tissue. *J. Biomed. Opt.* **2010**, *15*, 037001. [CrossRef] [PubMed]
15. Kazanci, M.; Wagner, H.D.; Manjubala, N.I.; Gupta, H.S.; Paschalis, E.; Roschger, P.; Fratzl, P. Raman imaging of two orthogonal planes within cortical bone. *Bone* **2007**, *41*, 456–461. [CrossRef]

16. Kazanci, M.; Roschger, P.; Paschalis, E.P.; Klaushofer, K.; Fratzl, P. Bone osteonal tissues by Raman spectral mapping: Orientation-composition. *J. Struct. Biol.* **2006**, *156*, 489–496. [CrossRef]
17. Wurm, A.; Kuhn, J.; Kugel, K.; Putzer, D.; Pallua, J.D. Raman microscopic spectroscopy as a diagnostic tool to detect *Staphylococcus epidermidis* in bone grafts. *Spectrochim. Acta Part A Mol. Biomol. Spectrosc.* **2022**, *280*, 121570. [CrossRef]
18. Kellgren, J.H.; Lawrence, J.S. Radiological assessment of osteo-arthrosis. *Ann. Rheum. Dis.* **1957**, *16*, 494–502. [CrossRef]
19. Takahashi, Y.; Sugano, N.; Takao, M.; Sakai, T.; Nishii, T.; Pezzotti, G. Raman spectroscopy investigation of load-assisted microstructural alterations in human knee cartilage: Preliminary study into diagnostic potential for osteoarthritis. *J. Mech. Behav. Biomed. Mater.* **2014**, *31*, 77–85. [CrossRef]
20. Thienpont, E.; Parvizi, J. A New Classification for the Varus Knee. *J. Arthroplast.* **2016**, *31*, 2156–2160. [CrossRef]
21. Buchwald, T.; Niciejewski, K.; Kozielski, M.; Szybowicz, M.; Siatkowski, M.; Krauss, H. Identifying compositional and structural changes in spongy and subchondral bone from the hip joints of patients with osteoarthritis using Raman spectroscopy. *J. Biomed. Opt.* **2012**, *17*, 017007. [CrossRef]
22. Kerns, J.G.; Gikas, P.D.; Buckley, K.; Shepperd, A.; Birch, H.L.; McCarthy, I.; Miles, J.; Briggs, T.W.R.; Keen, R.; Parker, A.W.; et al. Evidence from Raman spectroscopy of a putative link between inherent bone matrix chemistry and degenerative joint disease. *Arthritis Rheumatol.* **2014**, *66*, 1237–1246. [CrossRef] [PubMed]
23. Radin, E.L.; Paul, I.L.; Rose, R.M. *Role of Mechanical Factors in Pathogenesis of Primary Osteoarthritis*; Lancet: London, UK, 1972. [CrossRef]
24. Lehmann, T.P.; Filipiak, K.; Juzwa, W.; Sujka-Kordowska, P.; Jagodziński, P.P.; Zabel, M.; Głowacki, J.; Misterska, E.; Walczak, M.; Głowacki, M. Co-culture of human nucleus pulposus cells with multipotent mesenchymal stromal cells from human bone marrow reveals formation of tunnelling nanotubes. *Mol. Med. Rep.* **2014**, *9*, 574–582. [CrossRef] [PubMed]
25. Kobielarz, M.; Szostek, S.; Głowacki, M.; Dawidowicz, J.; Pezowicz, C. Qualitative and quantitative assessment of collagen an elastin in annulus fibrosus of the physiologic and scoliotic intervertebral discs. *J. Mech. Behav. Biomed. Mater.* **2016**, *62*, 45–56. [CrossRef] [PubMed]
26. Bobinac, D.; Spanjol, J.; Zoricic, S.; Maric, I. Changes in articular cartilage and subchondral bone histomorphometry in osteoarthritic knee joints in humans. *Bone* **2003**, *32*, 284–290. [CrossRef]
27. Bruyere, O.; Dardenne, C.; Lejeune, E.; Zegels, B.; Pahaut, A.; Richy, F.; Seidel, L.; Ethgen, O.; Henrotin, Y.; Reginster, J.-Y. Subchondral tibial bone mineral density predicts future joint space narrowing at the medial femoro-tibial compartment in patients with knee osteoarthritis. *Bone* **2003**, *32*, 541–545. [CrossRef]
28. Głowacki, M.; Ignys-O'Byrne, A.; Melzer, P.; Melzer, P. Evaluation of volume and solitary bone cyst remodelling using conventinal radiological examination. *Skelet. Radiol.* **2010**, *39*, 251–259. [CrossRef]
29. Głowacki, M.; Ignys-O'Byrne, A.; Wróblewska, K.; Ignys, I. Limb shortening in the course of solitary bone cyst treatment—A comparative study. *Skelet. Radiol.* **2011**, *40*, 173–179. [CrossRef]
30. Czarny-Ratajczak, M.; Biegański, T.; Głowacki, M.; Kozłowski, K. New Intermediate Phenotype Between MED and DD Caused by Compound Heterozygous Mutations in the DTDST Gene. *Am. J. Med. Genet. Part A* **2010**, *152*, 3036–3042. [CrossRef]
31. Timlin, J.A.; Carden, A.; Morris, M.D. Chemical Microstructure of Cortical Bone Probed by Raman Transects. *Appl. Spectrosc.* **1999**, *53*, 1429–1435. [CrossRef]
32. Schmidt, V.M.; Zelger, P.; Wöss, C.; Huck, C.W.; Arora, R.; Bechtel, E.; Stahl, A.; Brunner, A.; Zelger, B.; Schirmer, M.; et al. Post-Mortem Interval of Human Skeletal Remains Estimated with Handheld NIR Spectrometry. *Biology* **2022**, *11*, 1020. [CrossRef]